Ceramics International 51 (2025) 2695–2700

Contents lists available at ScienceDirect

Ceramics International

journal homepage: www.elsevier.com/locate/ceramint

Neutron irradiation induced transmuted Ga-doping of ZnO thin films: Structural and opto-electronic investigations

Saideep Shirish Bhat [a], Shivakumar Jagadish Shetty [a], M.P. Shilpa [a,d], Sachin Shet [b], K.M. Eshwarappa [c], S.C. Gurumurthy [a,*]

[a] Nano and Functional Materials Lab (NFML), Department of Physics, Manipal Institute of Technology, Manipal Academy of Higher Education, Manipal, 576104, Karnataka, India
[b] Manipal Centre for Natural Sciences, Manipal Academy of Higher Education, Manipal, 576104, Karnataka, India
[c] Radiation and Material Physics Lab, Department of Studies in Physics, Davanagere University, Shivagangothri, Davanagere, 577007, Karnataka, India
[d] Post Graduate Department of Physics, St Philomena College (Autonomous), Puttur, 574202, Karnataka, India

ARTICLE INFO

Handling Editor: Dr P. Vincenzini

Keywords:
Spin coating
Metal oxide
Beta decay
Zinc
Gallium
Nuclear transmutation doping

ABSTRACT

Metal oxide nanoparticles, particularly zinc oxide (ZnO) thin films, have significant applications in photocatalysis, non-volatile memories, resistive switching, energy conversion, and many more. This study examines the effects of neutron irradiation on ZnO thin films synthesized via a sol-gel and spin coating technique, subsequently annealed at 450 °C. The films are exposed to neutron radiation of various fluence rates. One of the major effects of neutron irradiation is the transmutation of zinc (Zn) into gallium (Ga), resulting in a Ga-doped ZnO thin film. Scanning electron microscopy (SEM) reveals morphological changes, including forming nano-scale structures on the surface, post-irradiation. Energy dispersive X-ray analysis (EDAX) identifies the transmutation of Zn to Ga. X-ray diffraction indicates a shift in the peaks due to radiation-induced defects. Optical studies show a blue shift in absorption spectra and an increase in bandgap from 3.1 eV to 3.2 eV after irradiation. Photoluminescence spectra exhibit intensified defect-related emissions. Electrical measurements via I-V and Hall techniques reveal reduced current and carrier concentrations with transmuted Ga-doped ZnO thin film. These findings highlight the significant impact of neutron irradiation on the structural, optical, and electrical properties of ZnO thin films, providing insights into their behaviour under space-like conditions.

1. Introduction

In the mid-1950s, the exploration of ZnO marked a significant milestone in scientific and industrial research. Its properties, such as piezoelectricity, luminescence, ultraviolet (UV) absorption, and catalytic activity, positioned ZnO as a versatile material for diverse applications across various industries. ZnO's high melting point of 2248 K and a substantial cohesive energy of 7.5 eV underscores its robustness as a semiconducting material. Additionally, its direct and wide band gap of 3.10–3.37 eV at room temperature makes ZnO a desirable choice for optical device applications. Despite ZnO's poor solubility in water, its high solubility in alkalis and acids makes it easier to fabricate thin films [1,2]. The hexagonal wurtzite structure of ZnO, characterized by alternating planes of tetrahedrally coordinated O^{2-} and Zn^{2+} ions along the c-axis, combined with its non-toxic nature and environmental abundance, further heightens its attractiveness for extensive exploration [3].

Experiments involving particulate and electromagnetic radiation have been employed for decades to investigate the effects of radiation on materials. These types of radiation, including protons, electrons, gamma rays, and neutrons, can induce alterations in structural, morphological, optical, and electrical properties, individually imparting distinct effects [4–7]. Beyond its inherent material properties, ZnO is an exemplary model for studying the impact of irradiation-induced defects. ZnO thin films have been subjected to ionizing and non-ionizing radiations to tune their structure and properties and enhance their effectiveness for specific applications [8].

Proton irradiation generally induces point defects and clusters. However, due to the limited penetration depth, proton defects often manifest only on the surface, restricting their utility in specific applications. In contrast, neutron irradiation leads to more severe defect structures, such as cluster defects, owing to the high penetration depth [9]. When neutrons interact with materials, they primarily collide with

* Corresponding author.
E-mail address: gurumurthy.sc@manipal.edu (S.C. Gurumurthy).

https://doi.org/10.1016/j.ceramint.2024.11.252
Received 18 August 2024; Received in revised form 11 November 2024; Accepted 16 November 2024
Available online 17 November 2024

the nucleus, generating a high-energy state. This results in enhanced structural and morphological impact compared to high-energy protons. The involvement of excited nuclei by neutron irradiation in the reaction is crucial, highlighting the high linear energy transfer [10]. Hence, out of various irradiation methods, the neutron irradiation method stands superior because it can initiate nuclear transmutation within the sample. This process is also effective for material doping. ZnO can be doped using several techniques. Buzok et al. used the sol-gel method to dope ZnO with cobalt, examining its structural, optical, and electrical properties [11]. Demircan et al. doped silicon and titanium to ZnO using sol-gel techniques [12]. Using a co-sputtering technique, Appani et al. coated a Ga-doped ZnO thin film [13]. Wang et al. doped Ga to ZnO using the hydrothermal method and used it for the detection of butanol [14]. A different approach is used here, especially for doping ZnO with p-block elements like Ga. Zn can undergo transmutation into Ga and copper (Cu) by neutron capture, followed by beta decay and electron capture, respectively, which is known as nuclear transmutation doping (NTD). Doping elevates material properties, and incorporating Ga into ZnO explicitly improves the electrical properties of the films [15]. Dopant atoms replace the Zn in the films, potentially increasing the density of free electrons, carrier concentration, or both. The smaller ionic radius of Ga^{3+} (0.62 Å) compared to Zn^{2+} (0.74 Å) and the shorter covalent bond length for Ga–O (1.92 Å) compared to Zn–O (1.97 Å) favour the effective doping of Ga in ZnO films [16,17].

While NTD offers several advantages, such as precise control over doping concentration and uniformity, there are several limitations and potential drawbacks associated with this method. NTD, when very high flux is necessary, requires nuclear reactors, which are expensive to operate and maintain. The infrastructure for performing this method is limited to facilities with nuclear reactors, making it costlier than other doping methods like chemical vapor deposition or ion implantation. Handling radioactive materials and exposure to neutron flux requires stringent safety measures and regulations, which add to the operational complexity and costs. Compared to other doping techniques, the process is not easily scalable, limiting its practicality for mass production in industries. Post-irradiation, samples may retain some radioactive isotopes temporarily. While these isotopes decay over time, handling the material immediately after irradiation requires careful attention to safety and potential environmental concerns. Achieving uniform doping takes time, as neutrons need to irradiate the samples over a prolonged period. Exposure to high-energy neutrons can create defects in the lattice, such as vacancies and interstitials. These defects can negatively impact the electrical properties of the material if not treated adequately through annealing [18].

Despite this, numerous studies have explored the irradiation of ZnO by neutrons. Zhao et al. irradiated ZnO nanowires and nanoflakes with a neutron flux of 10^{15} n/cm^2/s. Post-irradiation, the nanowires exhibited reduced diameters, and nanoflakes transformed into nanoparticles. Photoluminescence analysis revealed a red shift in the near-band emission, indicating shallow defects [19]. Kim et al. subjected ZnO thin films to thermal and fast neutron irradiation for 0.5, 24, and 168 h with 6.73 x 10^{13} and 1.0 x 10^{11} n/cm^2/s flux rates, respectively. Photoluminescence measurements confirm the formation of Cu, although Ga's presence is inconclusive due to its low concentration [20]. Selim et al. used NTD to incorporate Cu into ZnO, confirming Cu^{2+} presence through infrared absorption [21]. Zeidan et al. observed an increase in photoluminescence intensity of the Ga exciton line after 12 days of continuous slow neutron irradiation on a ZnO single-crystal [22]. However, the investigation of ZnO's NTD needs to be explored further. Notably, much of the literature lacks detailed elemental analysis to confirm the presence of dopants (transmuted atoms).

The present study employs a simple spin-coating technique to fabricate the ZnO thin films, which are then irradiated by neutrons using an isotopic Americium-Beryllium (Am-Be) source to observe the structural and morphological transformation. Elemental mapping confirms the transmutation of Zn into Ga. The optical and electrical properties of irradiated and unirradiated films are systematically compared. This approach provides insights into the fundamental processes and enhances the broader understanding of ZnO's behaviour under neutron irradiation, offering potential applications in various technological advancements.

2. Experimental details

2.1. Materials

Zinc acetate dihydrate ($(CH_3COO)_2Zn.2H_2O$, 98%) was procured from Emplura, Merck Life Science Private Limited. Ethanol (C_2H_5OH, 99.9%) was purchased from Absolute Analytical CS Reagent. Monoethanolamine (C_2H_7NO, 99%) was procured from Isochem Laboratories. Iso-Propyl Alcohol (IPA) (C_3H_8O, 99%) and acetone (C_3H_6O, 99%) were procured from Loba Chemie Private Limited.

2.2. Synthesis of ZnO films

The ZnO thin films were fabricated by sol-gel technique using zinc acetate dihydrate and ethanol as precursors and solvents, respectively. The stabilizer monoethanolamine favoured the formation of sol-gel. A solution was prepared by combining zinc acetate dihydrate and monoethanolamine in a 1:1 ratio in ethanol with continuous stirring at a temperature of 60 °C for 30 min. Glass substrate was cleaned subsequently using ultrasonication in milli Q water, acetone, and isopropyl alcohol each for 10 min, followed by drying. The resulting film was fabricated by coating the solution on the substrate utilizing the spin-coating technique at 2000 rpm for 30 s and subsequently dried using a hot plate at 180 °C. This coating process was iteratively conducted 12 times to achieve the film thickness of 560 nm. The prepared films underwent post-annealing at a temperature of 450 °C for an hour.

2.3. Neutron irradiation of prepared thin films

The prepared ZnO thin films were irradiated with neutrons using a 16 Curie (Ci) Am-Be white spectrum neutron source with a 3.5 x 10^7 n/s yield in an isotropic direction. The distance between the source and the set of samples was maintained at 10 cm. The source gives a constant fluence rate of 5×10^3 n/cm^2/s at the irradiation location. The thin films with the corresponding fluence rates were retrieved at 15- and 30-day intervals, as indicated in Table 1.

2.4. Characterization techniques

X-ray diffraction (XRD) was utilized to investigate the structure of the thin film using Rigaku Miniflex powder XRD unit, employing Cu-Kα radiation with a wavelength of 1.54 Å. The spectrum was systematically recorded over a 20°–80° range of 2Θ, maintaining a step size of 0.02°. Surface morphology analysis involved SEM with a Carl Zeiss Sigma Microscope, operated at an applied accelerating voltage of 10 kV. Compositional studies were conducted through EDAX, utilizing an Oxford X-act detector integrated into the SEM apparatus. The optical studies of the films were captured using a SHIMADZU- 1900i UV–VIS spectrophotometer within the range of 190–1100 nm. Further investigations included a room-temperature photoluminescence study using a Jasco FP-8500 spectrofluorometer, incorporating a 305 nm excitation wavelength. A Bruker Dektak XT stylus profilometer was

Table 1
Fluence rate of irradiated samples.

Sample Name	Fluence Rate (n/cm^2/s)	Days
ZN_0	0	0
ZN_1	6.48×10^9	15
ZN_2 (transmuted Ga-doped ZnO film)	12.96×10^9	30

employed to determine film thickness, and it was measured to be 560 nm for the synthesized films. The electrical parameters of the thin films were investigated using the Van der Pauw configuration, integrating a Keithley 2450 source meter. A 0.6 T magnetic field was applied using electromagnets during the Hall effect measurements and conducted at room temperature. This multifaceted approach contributes to thoroughly understanding the material's structural, morphological, optical, and electrical characteristics.

3. Results and discussions

The transmutation of Zn to Ga in ZnO can be explained by the following equations.

$$ {}^{1}_{0}n + X^{A}_{Z} \rightarrow X^{A+1}_{Z} \quad (1) $$

$$ X^{A+1}_{Z} \rightarrow Y^{A+1}_{Z+1} + {}^{0}_{-1}\beta + \Upsilon \quad (2) $$

Z is the atomic number, A is a mass number, X is the parent nucleus (Zn isotope), and Y is a daughter nucleus (Ga isotope).

Here, equations (1) and (2) represent the formation and the decay of an unstable nucleus (Nuclear Transmutation), respectively, to form a stable nucleus with a higher atomic number. Zn has five isotopes: ^{64}Zn, ^{66}Zn, ^{67}Zn, ^{68}Zn, and ^{70}Zn. Out of these, only two isotopes, ^{68}Zn and ^{70}Zn can transmute Zn to Ga. The nuclear transmutation of ^{64}Zn to ^{65}Cu is insignificant in the present study, as the half-life of ^{65}Cu is 243.93 days.

$$ {}^{68}_{30}Zn + {}^{1}_{0}n \rightarrow {}^{69}_{30}Zn \quad (3) $$

$$ {}^{69}_{30}Zn \rightarrow {}^{69}_{31}Ga + {}^{0}_{-1}\beta \quad (4) $$

$$ {}^{70}_{30}Zn + {}^{1}_{0}n \rightarrow {}^{71}_{30}Zn \quad (5) $$

$$ {}^{71}_{30}Zn \rightarrow {}^{71}_{31}Ga + {}^{0}_{-1}\beta + \gamma \quad (6) $$

As shown in equations (3) and (4), the stable isotope ^{68}Zn absorbs a neutron, transforming into an unstable isotope ^{69}Zn, with a half-life of 56.4 min. Subsequent transformations led to the creation of the stable isotope ^{69}Ga by beta decay. A parallel sequence of reactions occurred (equations (5) and (6)) with the ^{70}Zn isotope. However, the isotope ^{71}Zn exhibited a shorter half-life of 2.45 min, resulting in the formation of ^{71}Ga, as depicted in the equations above [22].

X-ray diffraction was carried out to evaluate the changes in the structure between unirradiated and irradiated films, as depicted in Fig. 1. The peaks reveal that the ZnO has a hexagonal wurtzite structure.

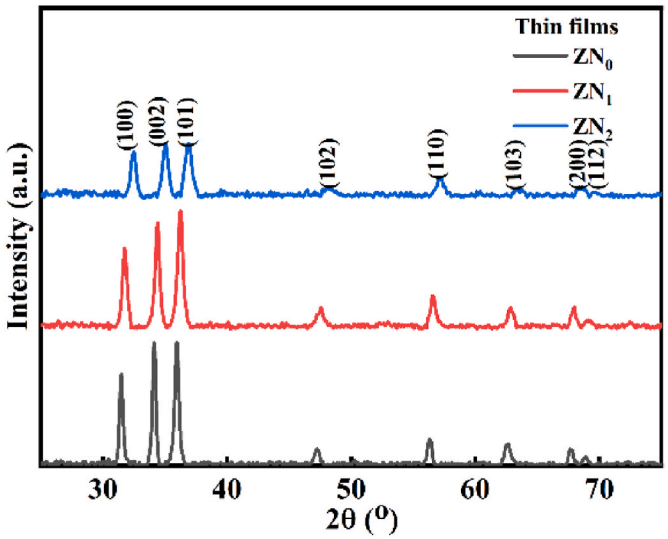

Fig. 1. X-ray diffraction pattern of ZN_0, ZN_1, and ZN_2 thin films.

The 2θ peaks of unirradiated ZnO thin films were observed at 31.5°, 34°, 35.9°, 48°, 57°, 63.4°, and 68.6° with corresponding planes (100), (002), (101), (102), (110), (103), and (112) which is in line with the international centre for diffraction data (ICDD) 00–036-1451 [23]. Post-irradiated ZnO thin films showed defects in the films and a shift in the peaks to the higher angles of 2θ by 0.7° and 1° for ZN_1 and ZN_2 films, respectively, compared to unirradiated ZnO thin films. In the ZN_2 thin films, no noticeable peak corresponding to Ga was noticed, and the shift in the peak was observed, showcasing the successful transmutation of Zn by Ga. Initially, when the ZnO thin film (ZN_1) is irradiated with neutrons, these neutrons interact with the ZnO lattice, causing lattice distortions, resulting in a peak shift of 0.7°. With increased irradiation time (ZN_2), transmutation of Zn to Ga occurs, as confirmed by EDAX analysis. In this case, the ionic radius decreases from 0.74 Å (Zn) to 0.68 Å (Ga) enhancing microstrain from 4.3×10^{-3} to 6.5×10^{-3} within the crystal as calculated using equation (8). This reduction in ionic radius causes lattice contraction and a shift in the peak to higher 2θ values, from 0.7° to 1°. Similar structural changes have been observed for Ga doping in ZnO in the literature, showcasing no Ga peaks in XRD pattern [24,25].

The crystallite size has been calculated using the Debye-Scherer equation:

$$ D = \frac{k\lambda}{\beta \cos\theta} \quad (7) $$

Also, microstrain is calculated using the formula:

$$ \varepsilon = \frac{\beta}{4 \tan\theta} \quad (8) $$

where D, λ, θ, β, k, and ε were crystallite size, X-ray radiation wavelength, Bragg's angle, full width at half maximum of the peaks, and a constant (0.9), respectively. The crystallite size was 27 nm, 20 nm, and 15 nm for ZN_0, ZN_1, and ZN_2, respectively. Post neutron irradiation, the peak intensity has reduced drastically due to the defects formed in the structure.

Further morphology analysis was conducted to study the induced surface changes during the neutron irradiation, as shown in Fig. 2. Fig. 2 (a)–(c) depicts the SEM images of ZN_0, ZN_1, and ZN_2 thin films. The unirradiated film (ZN_0) exhibits wrinkled shapes resulting from post-annealing. According to reports, thermal expansion of the substrate occurs during annealing. Further, the films undergo expansion without encountering thermal stress, aiming to reach the desired thickness and density. As the film undergoes cooling, it becomes denser, contracts, and accumulates compression stress, ultimately forming wrinkles [26]. After neutron irradiation, distinctive nano-scale spherical-like structures were observed to spread across the entire film. This phenomenon was particularly noticeable in the ZN_2 thin film sample. The neutron induces the migration of atoms from the surface, creating extensive vacancies in ZnO. This process suggests that the migration of ZnO atoms fosters the formation of nanoparticles [19]. Elemental composition analysis through EDAX confirmed the presence of Zn and O elements in the films (Fig. 2 (d)–(f)). Notably, ZN_2 thin film exhibits the presence of Ga (as illustrated in Fig. 2(f)), which is also observed in XRD through the shift in the peak. This transformation indicates that isotopes ^{68}Zn and ^{70}Zn are transmuted into ^{69}Ga and ^{71}Ga through subsequent beta decay reactions, resulting in a Ga composition of approximately 1.32 wt% on the film's surface. To examine the elemental distribution, the elemental mapping of ZN_2 confirms the elements Zn, O, and Ga (Fig. 2 (g)–(i)).

The absorption spectra of the unirradiated and irradiated films are depicted in Fig. 3(a). The absorption edge, at 390 nm, is attributed to the intrinsic bandgap absorption of ZnO. Following irradiation, a discernible blue shift in the absorbance edge is observed, indicating the Burstein-Moss effect [27]. This shift correlates with an increase in defects observed in the photoluminescence spectra and a shift in the XRD peaks of the irradiated samples.

An absorption spectra analysis determined the optical band gap for unirradiated and irradiated ZnO films. This estimation employs a model

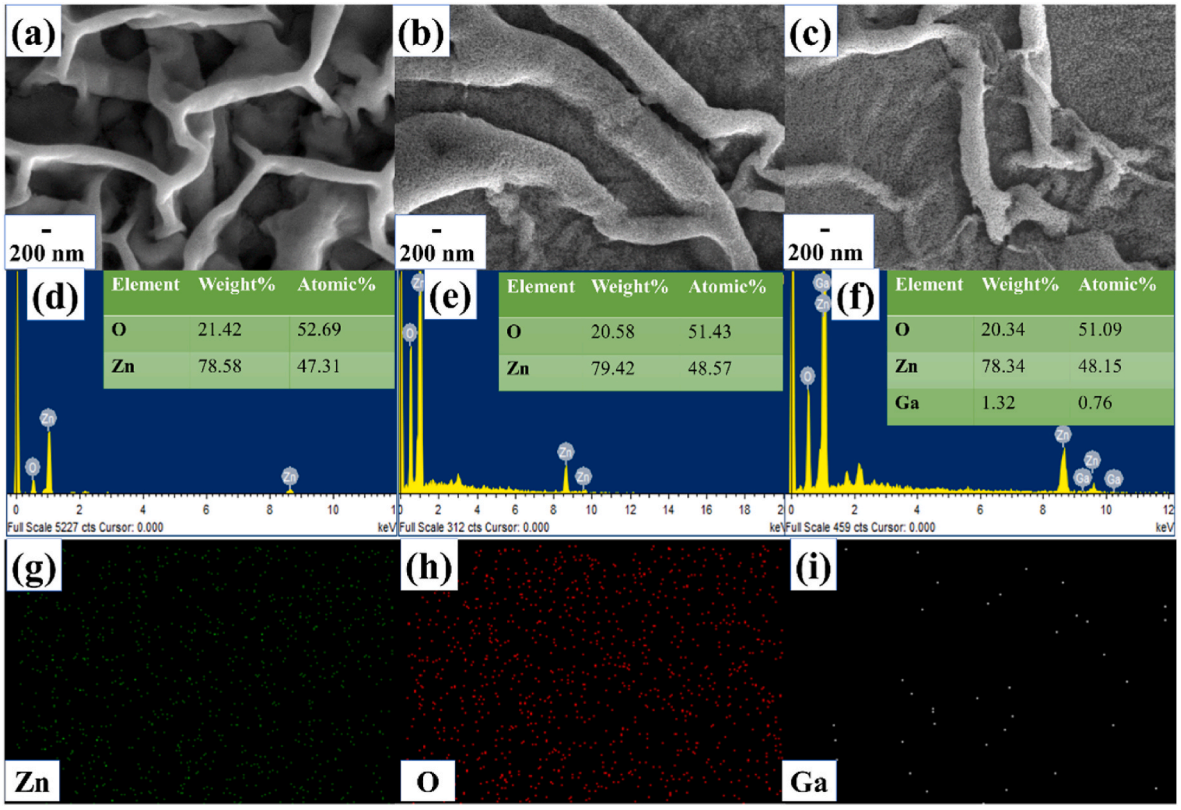

Fig. 2. (a–f) SEM, EDAX of ZN_0, ZN_1, and ZN_2, and elemental mapping of ZN_2 sample of the elements (g) Zn, (h) O, and (i) Ga.

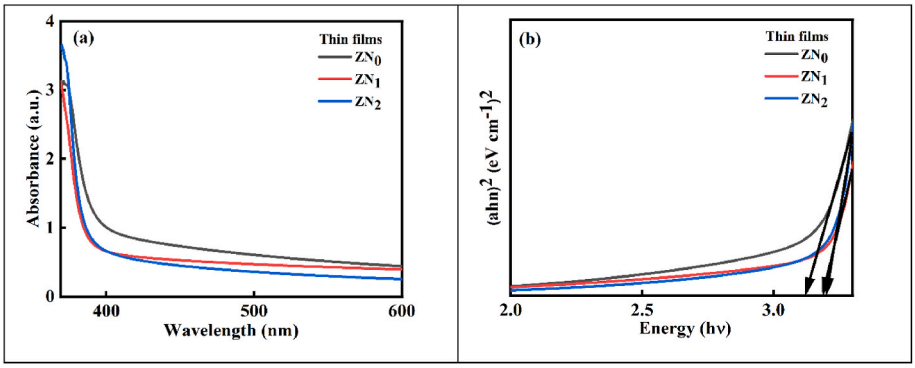

Fig. 3. (a) Absorbance spectra and (b) Tauc's plot of ZN_0, ZN_1, and ZN_2 thin films.

proposed by Tauc, represented by the equation:

$$(\alpha h\nu)^2 = A(h\nu - E_g) \quad (9)$$

where A is a constant, hυ denotes the photon energy, E_g is the optical band gap, and α represents the absorption coefficient [28]. Remarkably, observations indicate an increase in the band gap with irradiation, whereas the unirradiated ZnO thin film has a bandgap of 3.11 eV ZN_1 portrays a bandgap of 3.19 eV, while the transmuted Ga-doped ZnO thin film (ZN_2) sample exhibits a bandgap of 3.2 eV. The increase in the band gap can be predicted owing to the increase in defects, such as oxygen vacancies trapping down the charge carriers.

The photoluminescence spectra elucidate optical defects and relaxation pathways of excited states. Fig. 4 represents the room-temperature photoluminescence spectrum with an excitation wavelength of 305 nm. The peak at 398 nm is attributed to the recombination of excitons, which aligns with the band gap of the thin films. Additional peaks, originating from donor defect states like Zn interstitials (Zn_i) and oxygen vacancies (V_o), as well as acceptor defect states such as Zn vacancies (V_{Zn}) and oxygen interstitials (O_i), can be associated with these specific defect configurations. These defects are found to be minimal in ZN_0 thin film. Furthermore, the photoluminescence intensity increases with a further increase in neutron irradiation for ZN_1 and ZN_2 thin films. This may be due to the increased defects caused by neutron interaction with the ZnO lattice.

A peak observed near 421 nm is attributed to the transition between the levels of Zn_i and V_{Zn}. At this same position, a peak corresponding to doped Ga also appears, merging with the Zn_i-V_{Zn} transition in ZN_2. As a result, both transitions overlap at this point [29]. The blue emission spectra at 470 nm are ascribed to the transition from the ionized V_o (defect energy levels produced in the bandgap) to the valence band [30]. The blue-green emission intensity in the ZN_2 film has not significantly increased compared to the ZN_1 film. This is due to the presence of Ga, which occupies zinc lattice sites and reduces the probability of forming oxygen vacancies [31].Additionally, the peak at 566 nm in the green

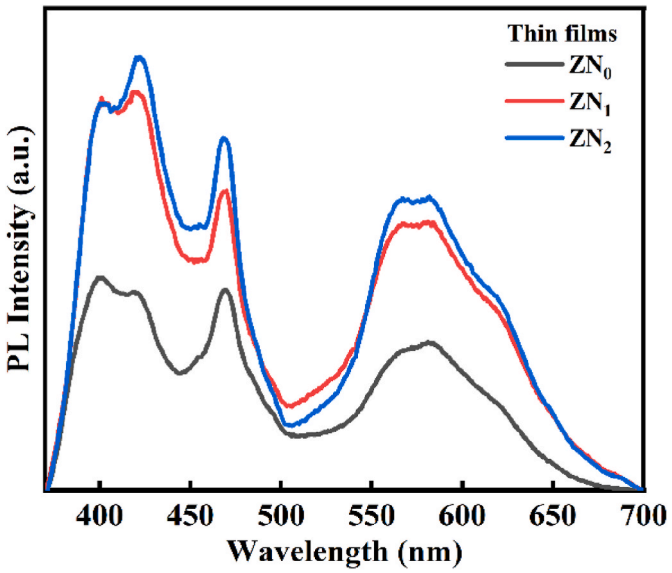

Fig. 4. Photoluminescence spectra of ZN_0, ZN_1, and ZN_2 thin films.

emission region is linked to oxygen vacancies generated during the transition from Zn_i to V_o [32]. The formation of deeply trapped, doubly charged oxygen vacancy (VO^{++}) states, formed by grain boundary-induced depletion regions, leads to radiative recombination with a conduction band electron. This yields photoluminescence at a wavelength of 564 nm [33]. Neutron irradiation of ZnO results in a higher level of induced defects in the material, which was also reflected in the XRD pattern of thin films showcasing shifts in the peaks.

The impact of neutron irradiation and transmuted Ga on the I–V characteristics of ZnO thin films is evaluated. Fig. 5 illustrates the I-V characteristics of both the neutron-irradiated and unirradiated samples. Upon irradiation, the reverse current decreased from 4.6 x 10^{-7} A to 1.1 x 10^{-8} A, and the forward current decreased from 4.1 x 10^{-7} A to 1.3 x 10^{-8} A. This behaviour change may be attributed to the increased band gap resulting from the observed rise in oxygen vacancies, evident in the green emission of the photoluminescence spectra. These oxygen vacancies are the charge traps that capture and immobilise charge carriers [34,35]. To further validate and understand this phenomenon, the carrier concentration of the thin films was calculated as 78 × 10^{15} cm^{-3}, 2.60 × 10^{14} cm^{-3}, and 7.18 × 10^{12} cm^{-3} for ZN_0, ZN_1, and ZN_2 thin films, respectively.

4. Conclusions

The ZnO thin films were successfully fabricated using sol-gel spin coating techniques and subjected to neutron irradiation from a 16 Ci Am-Be source to obtain Ga-doped ZnO thin films. The shift in the peaks due to the structural defects induced by neutron irradiation were investigated using XRD, demonstrating a decrease in intensity and crystallinity from 27 nm to 15 nm. Optical studies indicated a blueshift in the absorbance edge, with the bandgap of the samples increasing from 3.11 to 3.2 eV over the neutron irradiation period. The SEM images revealed distinctive wrinkles in the ZnO films. Post-irradiation, the samples tended to form more spherical nanostructures over the film. The elemental analysis confirmed the doping of transmuted Ga in the samples irradiated with a fluence rate of 12.96 × 10^9 $n/cm^2/s$. Photoluminescence studies revealed an augmentation of defects, such as oxygen vacancies, leading to electron trapping and making the film more resistive. Hall measurements showed a decrease in carrier charge i.e., 78 × 10^{15} cm^{-3}, 2.60 × 10^{14} cm^{-3}, and 7.18 × 10^{12} cm^{-3} for ZN_0, ZN_1, and ZN_2, respectively. Neutron irradiation not only transmuted elements but also significantly influenced the morphology, thereby

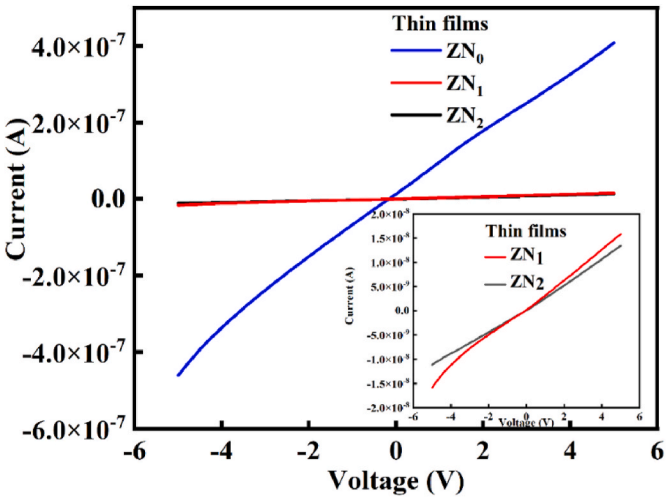

Fig. 5. I-V characteristics of ZN_0, ZN_1, and ZN_2 thin films (Inset: Enlarged image from 2.0x10^{-8} A to −2.0x10^{-8} A).

inducing the modifications of the characteristics of the ZnO films.

CRediT authorship contribution statement

Saideep Shirish Bhat: Writing – review & editing, Writing – original draft, Visualization, Methodology, Formal analysis, Data curation, Conceptualization. **Shivakumar Jagadish Shetty:** Writing – review & editing, Writing – original draft, Methodology, Formal analysis, Data curation, Conceptualization. **M.P. Shilpa:** Writing – review & editing, Writing – original draft, Methodology, Formal analysis, Data curation, Conceptualization. **Sachin Shet:** Writing – review & editing, Visualization, Validation, Methodology, Formal analysis. **K.M. Eshwarappa:** Writing – review & editing, Visualization, Formal analysis. **S.C. Gurumurthy:** Writing – review & editing, Visualization, Validation, Supervision, Formal analysis, Data curation, Conceptualization.

Statements and declarations

The authors declare that they have no conflict of interest.

Data availability

The data supporting this study's findings are available from the corresponding author upon reasonable request.

Declaration of competing interest

The authors declare that they have no known competing financial interests or personal relationships that could have appeared to influence the work reported in this paper.

Acknowledgements

All the authors acknowledge the invaluable support of their respective organizations. The authors thank Prof. (Dr) Sudha D. Kamath (MIT, Manipal) for providing photoluminescence spectra of the films (JASCO spectrofluorometer FP-8500-DST SERB). Saideep Shirish Bhat, Shivakumar Jagadish Shetty, Shilpa M P, Gurumurthy S C, and Sachin Shet acknowledge Manipal Academy of Higher Education for the funding facility.

References

[1] L.Y. Wang, B.Y. Shi, C.B. Yao, Z.M. Wang, X. Wang, C.H. Jiang, L.F. Feng, Y. L. Song, Size and morphology modulation in ZnO nanostructures for nonlinear optical applications: a review, ACS Appl. Nano Mater. 6 (2023) 9975–10014, https://doi.org/10.1021/ACSANM.3C01509.

[2] D. Das, P. Mondal, Photoluminescence phenomena prevailing in c-axis oriented intrinsic ZnO thin films prepared by RF magnetron sputtering, RSC Adv. 4 (2014) 35735–35743, https://doi.org/10.1039/C4RA06063F.

[3] Z.L. Wang, Zinc oxide nanostructures: growth, properties and applications, J. Phys. Condens. Matter 16 (2004) R829, https://doi.org/10.1088/0953-8984/16/25/R01.

[4] D. Sahoo, S. Sahoo, D. Alagarasan, R. Ganesan, S. Varadharajaperumal, R. Naik, Proton ion irradiation on as $_{40}$ Se $_{50}$ Sb $_{10}$ thin films: fluence-dependent tuning of linear–nonlinear optical properties for photonic applications, ACS Appl. Electron. Mater. 4 (2022) 856–868, https://doi.org/10.1021/acsaelm.1c01223.

[5] A. Sudha, S.L. Sharma, S.D. Sharma, Study of structural, optical and electrical properties of gamma irradiated In_2O_3 thin films for device applications, J. Mater. Sci. Mater. Electron. 28 (2017) 4619–4624, https://doi.org/10.1007/s10854-016-6100-2.

[6] M. Pattabi, S.C. Gurumurthy, G. Sanjeev, A.B. Gaikwad, Morphological changes in nanoparticulate silver films due to electron beam irradiation of polystyrene substrates, Nucl. Instrum. Methods Phys. Res. B 269 (2011) 1534–1539, https://doi.org/10.1016/j.nimb.2011.04.109.

[7] A.K. Sandhu, S. Singh, O.P. Pandey, Neutron irradiation effects on optical and structural properties of silicate glasses, Mater. Chem. Phys. 115 (2009) 783–788, https://doi.org/10.1016/j.matchemphys.2009.02.032.

[8] M.M. Zeidan, S. Abedrabbo, Enhancing photoluminescence spectra for doped ZnO using neutron irradiation, ACS Omega 8 (2023) 16722–16728, https://doi.org/10.1021/acsomega.3c00218.

[9] B.R. Gossick, Disordered regions in semiconductors bombarded by fast neutrons, J. Appl. Phys. 30 (1959) 1214–1218, https://doi.org/10.1063/1.1735295.

[10] D.K. Bewley, Calculated LET distributions of fast neutrons, Radiat. Res. 34 (1968) 437, https://doi.org/10.2307/3572568.

[11] E.B. Buzok, S. Yalcin, G. Demircan, D. Yılmaz, B. Aktas, E. Aytar, The structural, optical, electrical and radiation shielding properties of Co-doped ZnO thin films, Radiat. Phys. Chem. 222 (2024) 111840, https://doi.org/10.1016/j.radphyschem.2024.111840.

[12] G. Demircan, E.F. Gurses, B. Aktas, S. Yalcin, A. Acikgoz, G. Ceyhan, M.V. Balak, Sol–gel synthesis of Si-ZnO, Ti-ZnO and Si-Ti-ZnO thin films: impact of Si and Ti content on structural and optical properties, Mater. Today Commun. 34 (2023) 105234, https://doi.org/10.1016/j.mtcomm.2022.105234.

[13] S.K. Appani, D. Singh, R. Nandi, D.S. Sutar, S.S. Major, Influence of oxygen partial pressure on the strain behaviour of reactively co-sputtered Ga doped ZnO thin films, Thin Solid Films 764 (2023) 139624, https://doi.org/10.1016/j.tsf.2022.139624.

[14] T. Wang, J. Chen, J. Chen, X. Yao, G. Chen, Z. Jiao, J.-T. Zhao, S. Cheng, X.-C. Yang, Q. Li, UV-light enhanced gas sensor based on Ga doped ZnO for ultra-high sensitive and selective n-butanol detection, Appl. Surf. Sci. 641 (2023) 158551, https://doi.org/10.1016/j.apsusc.2023.158551.

[15] H. Kim, J.S. Horwitz, W.H. Kim, A.J. Mäkinen, Z.H. Kafafi, D.B. Chrisey, Doped ZnO thin films as anode materials for organic light-emitting diodes, Thin Solid Films (2002) 420–421, https://doi.org/10.1016/S0040-6090(02)00836-2, 539–543.

[16] J.K. Kim, J.M. Lee, J.W. Lim, J.H. Kim, S.J. Yun, High-performance transparent conducting Ga-doped ZnO films deposited by RF magnetron sputter deposition, Jpn. J. Appl. Phys. 49 (2010) 04DP09, https://doi.org/10.1143/JJAP.49.04DP09/XML.

[17] V.P. Verma, D. Kim, M. Jeon, W. Choi, Fabrication and characteristics of low doped gallium-zinc oxide thin film transistor, Mater. Res. Soc. Symp. Proc. 963 (2006) 222–227, https://doi.org/10.1557/PROC-0963-Q12-01/METRICS.

[18] N. Banaee, K. Goodarzi, H.A. Nedaie, Neutron contamination in radiotherapy processes: a review study, J. Radiat. Res. (2021) 947–954, https://doi.org/10.1093/jrr/rrab076.

[19] X. Zhao, Y. He, L. Chen, Neutron-irradiation effects on ZnO nanostructure, in: 2019 IEEE International Conference on Electron Devices and Solid-State Circuits (EDSSC), IEEE, 2019, pp. 1–2, https://doi.org/10.1109/EDSSC.2019.8754365.

[20] H. Kim, K. Park, B. Min, J.S. Lee, K. Cho, S. Kim, H.S. Han, S.K. Hong, T. Yao, Transmuted isotopes doped in neutron-irradiated ZnO thin films, Nucl. Instrum. Methods Phys. Res. B 217 (2004) 429–434, https://doi.org/10.1016/J.NIMB.2003.11.085.

[21] F.A. Selim, M.C. Tarun, D.E. Wall, L.A. Boatner, M.D. McCluskey, Cu-doping of ZnO by nuclear transmutation, Appl. Phys. Lett. 99 (2011), https://doi.org/10.1063/1.3662014/385158.

[22] A. Gulino, J. Eckert, M.M. Zeidan, S. Abedrabbo, Neutron irradiation to transmute zinc into gallium, Nanomaterials 13 (2023) 1487, https://doi.org/10.3390/NANO13091487, 2023.

[23] J.H. Bukhari, A.S. Khan, K. Ijaz, S. Zahid, A.A. Chaudhry, M. Kaleem, Low-temperature flow-synthesis-assisted urethane-grafted zinc oxide-based dental composites: physical, mechanical, and antibacterial responses, J. Mater. Sci. Mater. Med. 32 (2021) 1–11, https://doi.org/10.1007/S10856-021-06560-4.

[24] T. Prasada Rao, M.C. Santhosh Kumar, Physical properties of Ga-doped ZnO thin films by spray pyrolysis, J. Alloys Compd. 506 (2010) 788–793, https://doi.org/10.1016/j.jallcom.2010.07.071.

[25] O.A. Novodvorsky, L.S. Gorbatenko, V.Ya Panchenko, O.D. Khramova, YeA. Cherebilo, C. Wenzel, J.W. Bartha, V.T. Bublik, K.D. Shcherbachev, Optical and structural characteristics of Ga-doped ZnO films, Semiconductors 43 (2009) 419–424, https://doi.org/10.1134/S1063782609040034.

[26] B.R. Lee, E.D. Jung, J.S. Park, Y.S. Nam, S.H. Min, B.S. Kim, K.M. Lee, J.R. Jeong, R.H. Friend, J.S. Kim, S.O. Kim, M.H. Song, Highly efficient inverted polymer light-emitting diodes using surface modifications of ZnO layer, Nat. Commun. 5 (1 5) (2014) 1–8, https://doi.org/10.1038/ncomms5840, 2014.

[27] C.E. Kim, P. Moon, S. Kim, J.-M. Myoung, H.W. Jang, J. Bang, I. Yun, Effect of carrier concentration on optical bandgap shift in ZnO:Ga thin films, Thin Solid Films 518 (2010) 6304–6307, https://doi.org/10.1016/j.tsf.2010.03.042.

[28] O. Bazta, A. Urbieta, J. Piqueras, P. Fernández, M. Addou, J.J. Calvino, A. B. Hungría, Influence of yttrium doping on the structural, morphological and optical properties of nanostructured ZnO thin films grown by spray pyrolysis, Ceram. Int. 45 (2019) 6842–6852, https://doi.org/10.1016/J.CERAMINT.2018.12.178.

[29] H. Gupta, J. Singh, R.N. Dutt, S. Ojha, S. Kar, R. Kumar, V.R. Reddy, F. Singh, Defect-induced photoluminescence from gallium-doped zinc oxide thin films: influence of doping and energetic ion irradiation, Phys. Chem. Chem. Phys. 21 (2019) 15019–15029, https://doi.org/10.1039/C9CP02148E.

[30] A. Mahroug, B. Mari, M. Mollar, I. Boudjadar, L. Guerbous, A. Henni, N. Selmi, Studies on structural, surface morphological, optical, luminescence and UV photodetection properties of sol-gel Mg doped ZnO thin films 26 (2019), https://doi.org/10.1142/S0218625X18501676.

[31] S.S. Shinde, P.S. Shinde, Y.W. Oh, D. Haranath, C.H. Bhosale, K.Y. Rajpure, Structural, optoelectronic, luminescence and thermal properties of Ga-doped zinc oxide thin films, Appl. Surf. Sci. 258 (2012) 9969–9976, https://doi.org/10.1016/j.apsusc.2012.06.058.

[32] S.B. Zhang, S.H. Wei, A. Zunger, Intrinsic *n*-type versus *p*-type doping asymmetry and the defect physics of ZnO, Phys. Rev. B 63 (2001) 075205, https://doi.org/10.1103/PhysRevB.63.075205.

[33] J.D. Ye, S.L. Gu, F. Qin, S.M. Zhu, S.M. Liu, X. Zhou, W. Liu, L.Q. Hu, R. Zhang, Y. Shi, Y.D. Zheng, Correlation between green luminescence and morphology evolution of ZnO films, Appl. Phys. Mater. Sci. Process 81 (2005) 759–762, https://doi.org/10.1007/S00339-004-2996-0/METRICS.

[34] A. Indluru, K.E. Holbert, T.L. Alford, Gamma radiation effects on indium-zinc oxide thin-film transistors, Thin Solid Films 539 (2013) 342–344, https://doi.org/10.1016/J.TSF.2013.04.148.

[35] Z. Zhou, J. Liu, R. Long, L. Li, L. Guo, O.V. Prezhdo, Control of charge carriers trapping and relaxation in hematite by oxygen vacancy charge: ab initio non-adiabatic molecular dynamics, J. Am. Chem. Soc. 139 (2017) 6707–6717, https://doi.org/10.1021/JACS.7B02121.